

Improvement Physical Properties TiO₂ Thin Films by Mg Doping

Qasim Chfat Abdulridha

Ministry of Education/ General Directorate of Education in Qadisiya Governorate, Iraq.

Abeer Ghalib Hadi

Ministry of Education/ General Directorate of Education in Baghdad Governorate/ Rusafa second, Iraq.

Rana Talib Saihood

Ministry of Education/ General Directorate of Education in Baghdad Governorate/ Rusafa second, Iraq.

Nadir Fadhil Habubi

Department of Engineering of Refrigeration and Air Conditioning Technologies, Alnukhba University College, Iraq.

Sami Salman Chiad*

Department of Physics, College of Education, Mustansiriyah University, Iraq.

Abstract.

Chemical spray pyrolysis (CSP) method was utilized to make TiO₂ and TiO₂:Mg films. All of the samples were polycrystalline with anatase nanocrystalline structures, according to XRD research. With Mg doping, the crystallite size of TiO₂ increased from 14.29 nm to 18.09 nm. The average particle size of TiO₂ was 75.27 nm in AFM images, and the average particle size of (1, 3) percent Mg doped TiO₂ was 68.24 nm and 47.86 nm, respectively. The bandgap redshift has been observed in Mg doped TiO₂ thin films.

Keywords: TiO₂, Mg ,thin films, (CSP), Structure properties, surface topography.

Introduction

Titanium dioxide is an n-type, with a bandgap energy of 3.0 -3.2 eV. With the energy demands, solar cell fabrication using TiO₂ semiconductors is being investigated. Its relative abundance, low-cost, and non-toxicity have made it attractive to wide-ranging industrial applications. TiO₂ films are also used in the fabrication of solar cells for a variety of reasons, including high clarity in the UV–Vis field, high refractive indexes, and chemical composition stability [1, 2]. Due to its big bandgap, Pure TiO₂ only absorbs light in the ultraviolet (UV) spectrum (approximately 3.2 eV). Various modulation techniques, such as surface modification, have been used to transfer TiO₂'s absorption range to visible spectrum[3], size optimization [4,47-67], variation of composition for co-catalyst [5], and doping [6] have been pursued. Doping metals or non-metals into TiO₂ has been shown to change the visible spectrum's absorption range [7, 8]. Doping metals or non-metals into TiO₂ has a number of advantages, including narrowing the bandgap to absorb visible spectrum light, increased impurity energy levels, regulation of form, scale, and morphologies, and mitigation of recombination processes [9, 10]. Inserting metal ions into the TiO₂ structure is one of the most effective ways to boost TiO₂ optical properties [11,12]. Due to its costless, simplicity of preparation, and lack of toxicity, magnesium is an excellent choice for industrial applications. The ionic radii of Mg²⁺ (0.66Å) ions is analogous to Ti⁴⁺ (0.68 Å) ions. Therefore, these dopants will quickly replace Ti⁴⁺ in the TiO₂ matrix without causing structural changes. The purpose is to examine the influence of doping of Mg on pristine TiO₂ as the electrical and optical properties of semiconducting materials are substantially modified by impurity doping [13]. Sol–gel deposition [14], RF magnetron sputtering [15],

SILAR [16], CBD [17], and CSP [18-22] are some methods for preparing TiO₂ thin films that have been recorded. This paper aims to discuss the effect Mg on the optical properties, structure and surface topography of TiO₂ films prepared by CSP.

Experimental

CSP was used to make TiO₂ thin films. TiO₂ films are deposited from 0.1 M of (TiO₂Cl₂) dissolved in redistilled water. MgCl₂ dissolved in deionized water, HCl drops was joined to get clear solution. The optimal conditions was: Glass substrate temperature 450°C, space between spout and substrate was 28cm, spraying time 9s stopped for 60s to avert cooling, spray average was 5ml/min, and N₂ was employed as transporter gas. Thickness is gained by weighing method and was 330 ± 25 nm. Structural properties were investigated utilizing XRD in 2θ range from 20 to 70. AFM was used to implement surface topography. The UV–Vis spectrophotometer was used to get optical properties.

Results and discussion

XRD analysis (Shimadzu XRD 6000) was used to validate the structure and phases. Figure 1 displays the XRD trends. According to XRD, there is a pure anatase process as well as anatase, rutile, and brookite in a mixed phase. The peak corresponding to planes (120), (201), (132), (241), and (213) corresponds to the standard JCPDS card No (29-1660) of TiO₂'s anatase, rutile, and brookite (72-0100) process. The lack of Mg-related peaks is due to low number of metal ion dopants and Mg ion dispersion in TiO₂ lattices [23-25]. Peak density of Mg-doped TiO₂ polyscales was found to be higher in the XRD pattern causing well crystalline phases that appear to be stable and improve as Mg concentration is increased [26]. Scherrer's formula is employed to measure the crystallite size *D* [27-29]:

$$D = \frac{K\lambda}{\beta \cos\theta} \quad \text{--- --- --- 1}$$

Where, λ is the wavelength, β is FWHM, θ is the Bragg's angle and K is a constant (0.94). When Mg concentration is increased from 0 to 3 percent, *D* rises from 14.29 to 18.09 nm. The disparity in ionic radius and ionic charge between Mg²⁺ and Ti⁴⁺ is the reason for this and Mg²⁺ has a different ionic charge than Ti⁴⁺. As a result, Mg doping increases the number of oxygen vacancies in TiO₂ lattice to balance the charge [24]. A reduction in the lattice parameters is also shown by the peak change to higher angles [25].

The macrostrain ϵ was determined by using following relations [30-32].

$$\epsilon = \frac{\beta \cos\theta}{4} \quad \text{--- --- --- 2}$$

The dislocation density δ was determined by using following relations [33-35].

$$\delta = \frac{1}{D^2} \quad \text{--- --- --- 3}$$

As the crystallite size grows larger, the microstrain decreases as well. Table 1 summarizes the details of the structure, it is noted that the FWHM diffraction decreased and the intensity peaks were shifted slightly to the higher as Mg concentration rises.

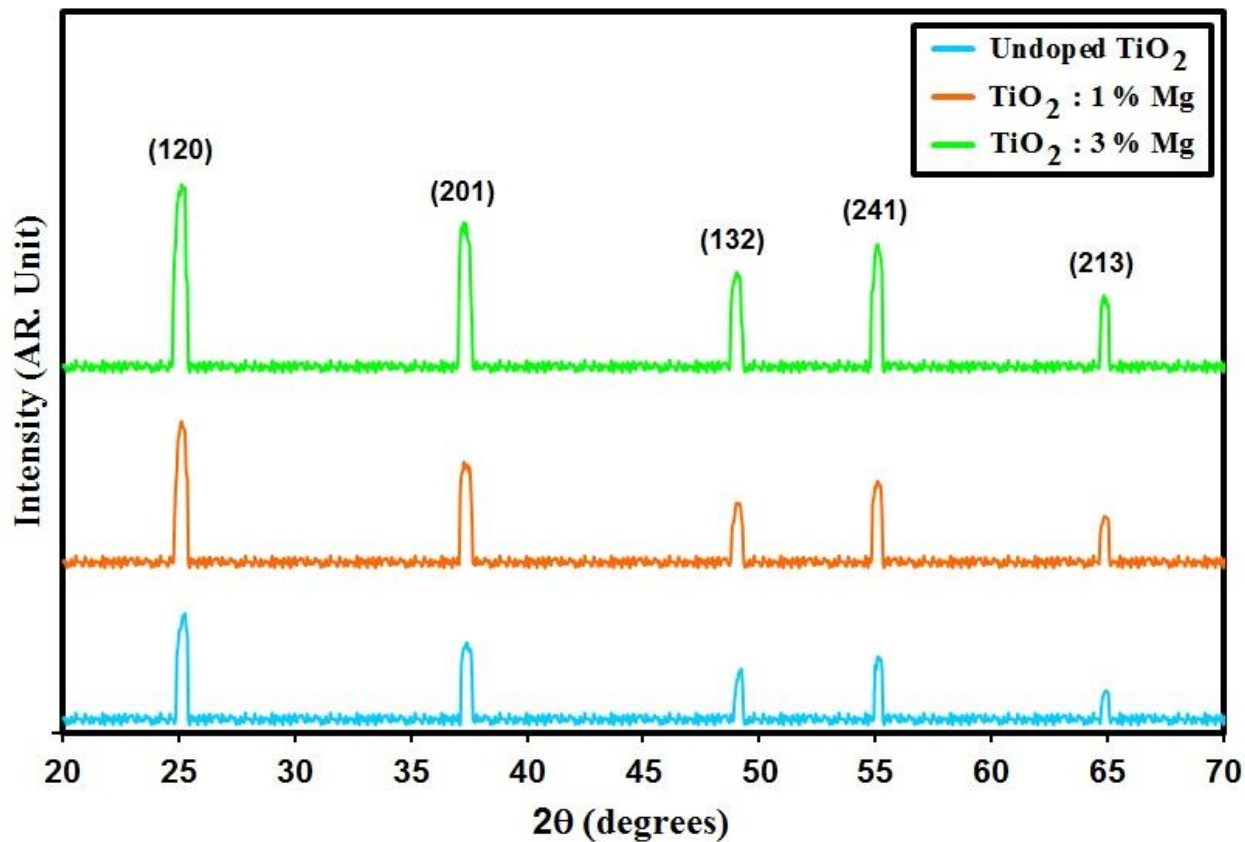


Fig.1. XRD styles of the grownfilms.

Table 1. XRD parameters of the intended films.

Specimen	2θ (°)	(hkl) Plane	FWHM (°)	Optical bandgap (eV)	crystallite size (nm)	Dislocations density ($\times 10^{15}$) (lines/m ²)	Strain ($\times 10^{-3}$)
Undoped TiO ₂	25.35	120	0.57	3.72	14.29	4.89	2.42
TiO ₂ : 1% Mg	25.31	120	0.51	3.68	16.00	3.90	2.17
TiO ₂ : 3% Mg	25.27	120	0.45	3.62	18.09	3.05	1.91

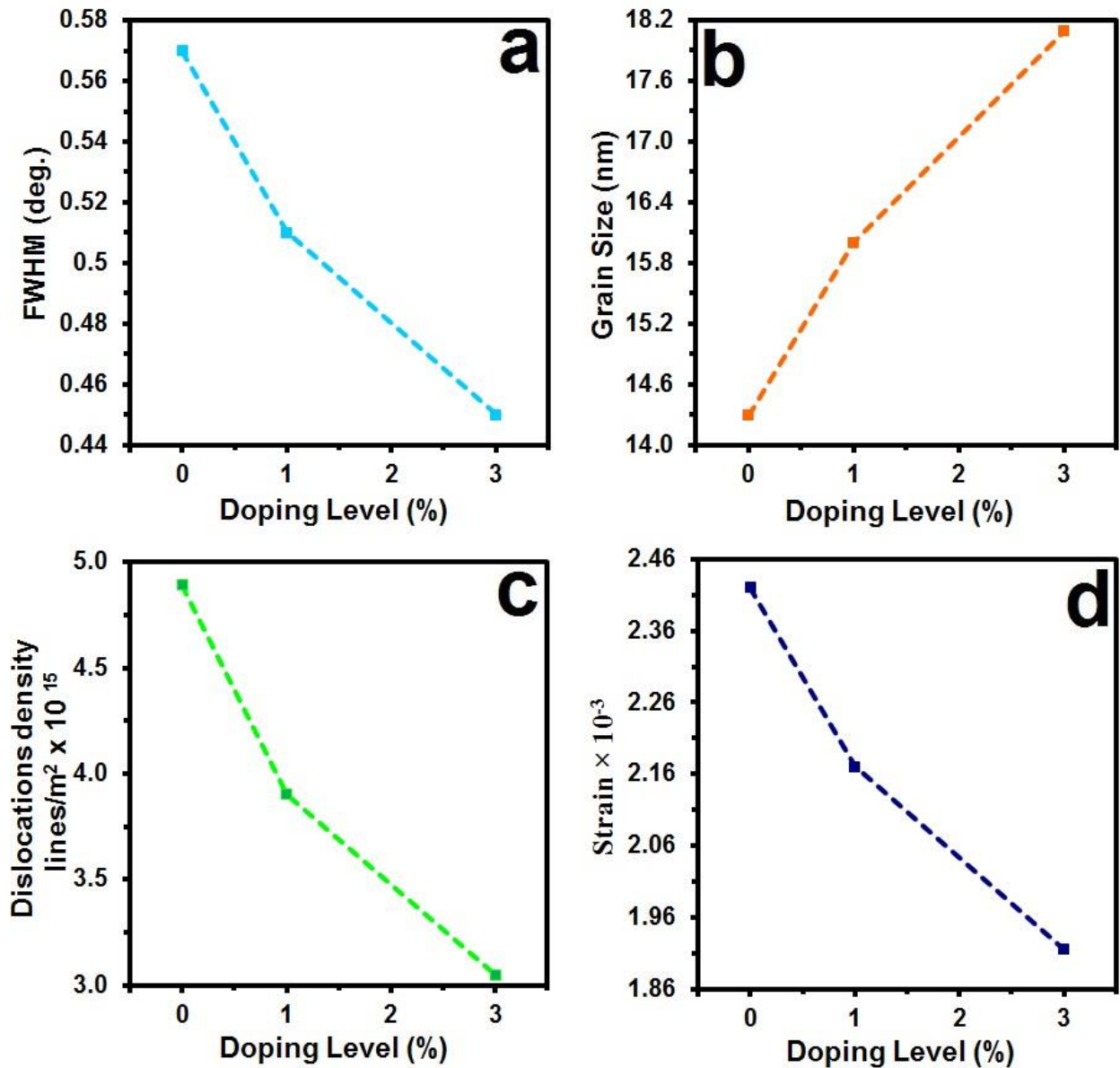


Fig. 2. X-ray parameter of the intended films.

AFM was used to examine the films' surface morphology. Fig. 3 displays 3-dimensional (AFM) images ($78 \times 78 \text{ nm}^2$) of the films prepared. We can see densely packed grains in the films with dissimilar grain sizes and uniform surface for different doping concentrations. The Surface Roughness Mean Square (RMS), as well as the roughness and average particle size P_{av} of these films, are all enough. The average particle size for pure films is 75.27 nm, with a smaller value of 47.86 nm for films doped in Mg 3 percent concentration. As the doping level is increased, the closely packed grain size shrinks, resulting in a decrease in RMS and roughness and an increase in surface uniformity. These film surfaces are made up closely packed grains that form a smooth, void-free base. The resulting AFM images demonstrate that the films have a nanocrystalline structure as summarized in table 2.

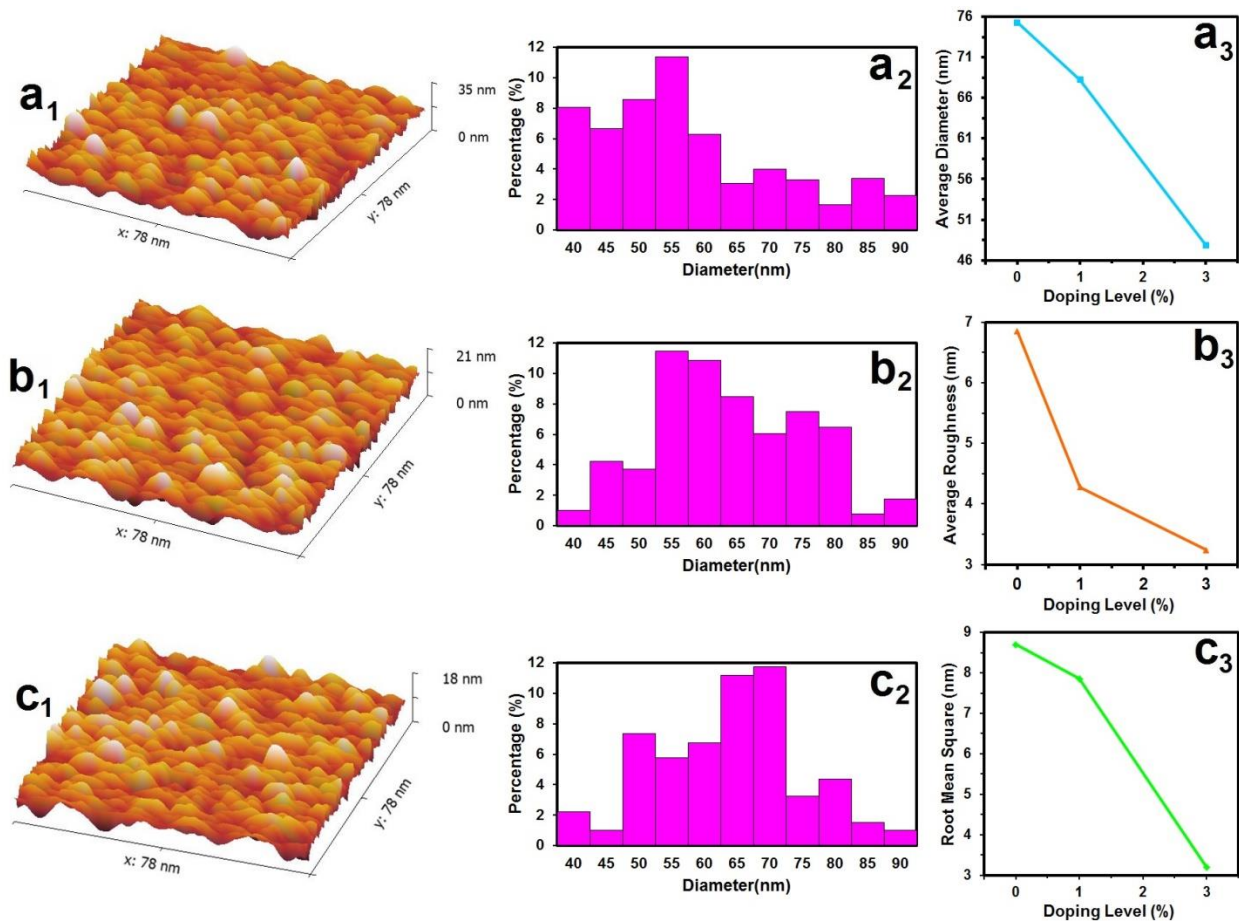


Fig.3. AFM of the intended films.

Table 2. AFM parameter of the intended films.

Samples	P_{av} nm	R_a (nm)	RMS (nm)
Undoped TiO_2	75.27	6.85	8.70
TiO_2 : 1% Mg	68.24	4.28	7.86
TiO_2 : 3% Mg	47.86	3.24	3.20

Between the wavelengths of 300 and 900 nm, the transmittance(T) spectra of the intended films were measured. The TiO_2 film deposited at 450°C has a gross transmittance of approximately 90%. The films' optical transmittance was deposited at various doping levels as seen in Figure 4. The transmittance decreased with higher doping levels, which may be due to variations in the surface morphology and microstructure of TiO_2 films.

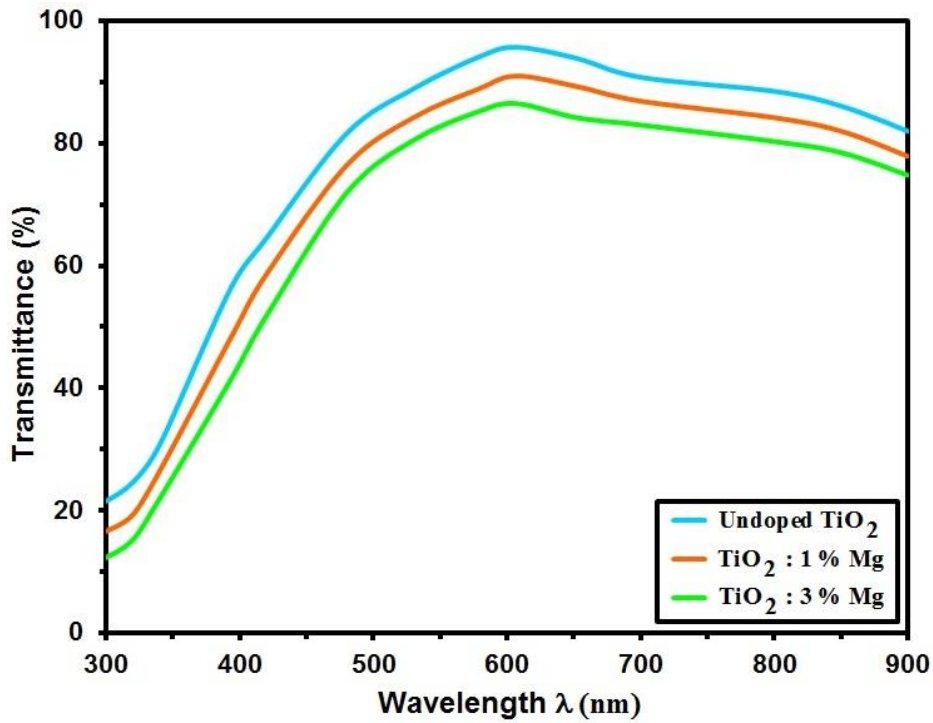


Fig.4. Transmittance of pure and TiO₂:Mg films with different dopant.

Equation (4) is employed to calculate the value of optical band gap (E_g) by determining the absorption coefficient (α) [36-38]:

$$\alpha = \frac{\ln(1/T)}{d} \quad \text{--- 4}$$

where T and d indicate the overall film transmittance and its thickness.

The absorption coefficient (α) is measured and plotted against $h\nu$ as depicted in fig. 5.

Figure 5. shows α of the intended films. The absorption coefficient (α) for Mg-doped films is greater than for undoped films at both ($h\nu$). Based on Burstein-Moss effect [39], the absorption edge shifts to a shorter wavelength as the Mg concentration is increased, which is associated with a rise in the concentration of carriers in the conduction band.

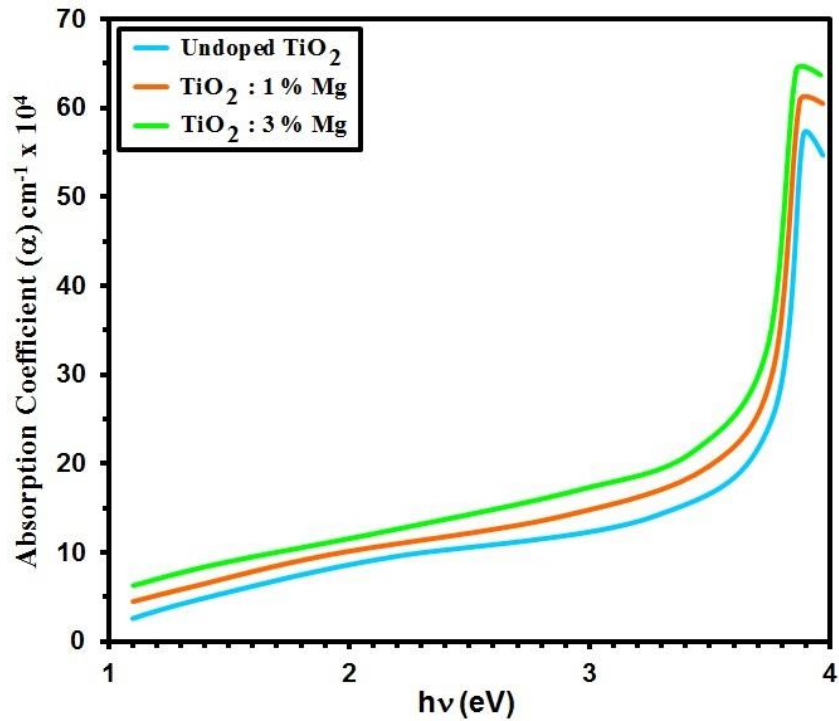


Figure 5. α with photon energy of pure and $\text{TiO}_2\text{:Zn}$ films with different dopant.

The band gap E_g was determined by using Tauc equation, where k is constant, $h\nu$ is the photon energy [40-42]:

$$(\alpha h\nu) = K(h\nu - E_g)^n \quad \text{----- 5}$$

The plot of $(\alpha h\nu)^2$ against $(h\nu)$ yielded the band gap values shown in Figure 6.

As the doping concentration increased, E_g values decreased. Mg doping has risen, resulting in the creation of new localized or donor levels. There is a shifted in absorption edge into longer wavelengths, resulting in a decrease in the optical energy gap's value. [43]

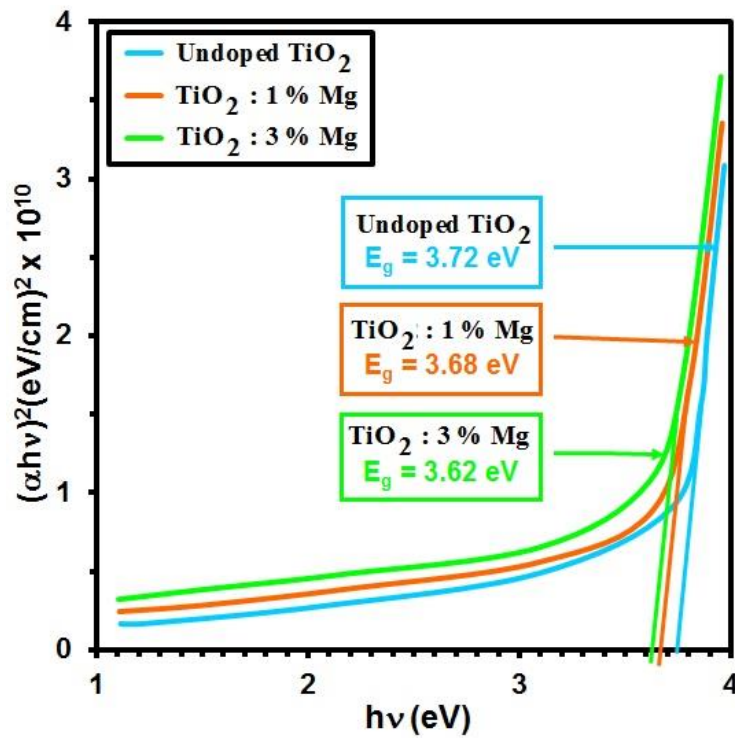


Fig. 6. E_g of pure and $TiO_2:Mg$ films with different dopant.

The refractive index (n) variance with wavelength dependency on the film developed at various substrate doping levels, and n was determined using equation (6) [44-45]:

$$n = \frac{\sqrt{1+R}}{\sqrt{1-R}} \quad \text{----- 6}$$

where R is the reflectance. Figure 7 shows the plot of the estimated value of n using Eq. 6. For both of the substrates, the refractive index n decreases as the wavelength rises. The graphs are representative of natural dispersion, in which the refractive index drops in the (600-900) nm range because of electronic inter-band absorption for photon energies higher than the smallest band difference in the ultra-violet field, which reaches into the visible region [46]. The refractive index increases as the concentration of Mg increases, as seen in Fig.7. As light is shone on a denser substrate with a higher refractive index, more electric dipoles are stimulated [46]. Equation 8 was used to determine the extinction coefficient (k) [47]:

$$k = \frac{\alpha\lambda}{4\pi} \quad \text{----- 7}$$

Figures 8 demonstrate the difference of the extinction coefficient (k) via λ . The extinction coefficient (k) reduces as wavelength changes in the visible area due to normal dispersion of films. TiO_2 thin film's excellent surface smoothness is shown by its low extinction coefficient in the near infrared as well as visible regions [48].

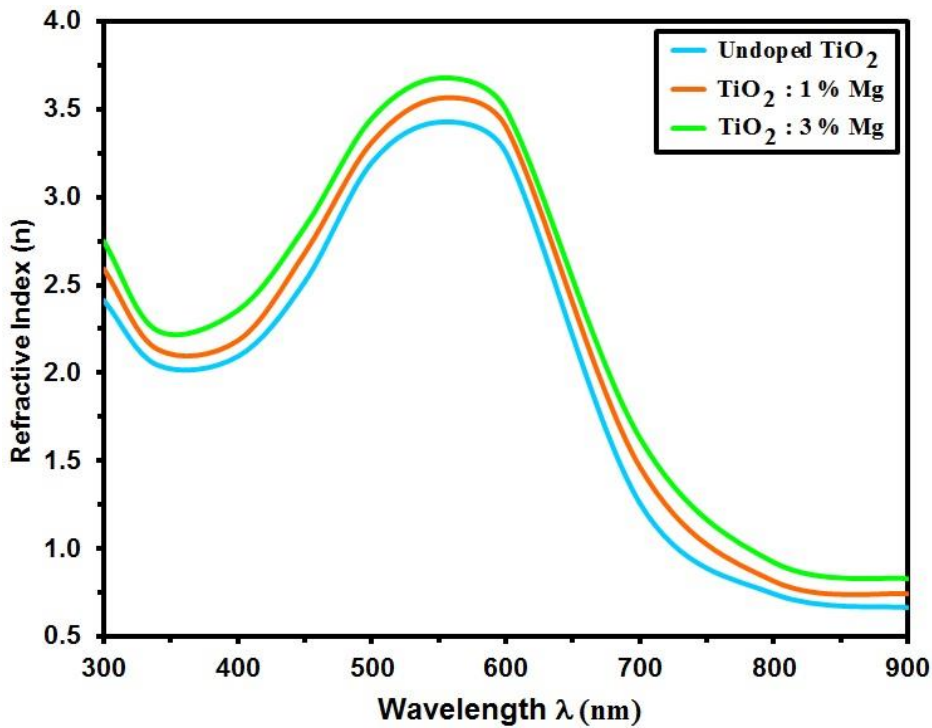


Figure 7. n of the intended films

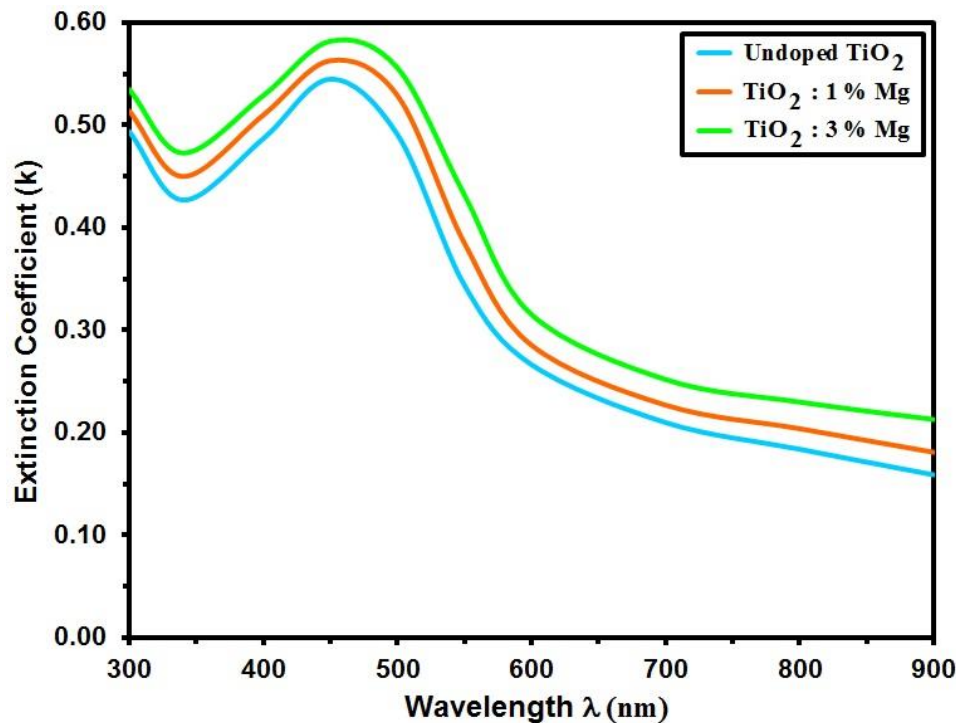


Figure 6. k of the intended films

Conclusion

The current study examined the grown of pure and TiO₂:Mg with different concentration have been prepared via CSP technique. The XRD findings showed that anatase and rutile have well-crystalline phases with stable and smaller polyscales. As the Mg concentration is increased from 0 to 3 percent M, the crystallite size grows from 14.29 to 18.09 nm. The AFM findings revealed that the films have a nanocrystalline composition and have a uniform topography. The transmittance decreased as the doping level increased, which may be due to variations in the TiO₂ films' microstructure and surface morphology. The band gap (E_g) values declined slightly as doping concentration increased.

Acknowledgments

Authors uphold Mustansiriyah University (www.uomustansiriyah.edu.iq) and Alnukhba University College for their support

References

- [1] Yanag Hisao, Ohoka Yoshihiro, Hishiki Takashi, Ajito Katsuhiro, Fujishima Akira, "Characterization of dye-doped TiO₂ films prepared by spray-pyrolysis," *Appl Surf Sci* 113/114:426–443(1997).
- [2] HMN Bandara, RMG Rajapakse, K. Murakami, GRRR Kumaraa, G. Anuradha Sepalage, "Dye-sensitized solar cell based on optically transparent TiO₂ nanocrystalline electrode prepared by atomized spray pyrolysis technique," *Electrochim. Acta*.56:9159–9161(2011).
- [3] L. Li, J. Liu, Y. Su, G. Li, X. Chen, X. Qiu, T. Yan, "Surface doping for photocatalytic purposes: relations between particle size, surface modifications, and photoactivity of SnO₂:Zn₂," *Nanotechnology*,55706(2009).
- [4] CB. Almquist, P. Biswas, " Role of synthesis method and particle size of nanostructured TiO₂ on its photoactivity," *J Catal* 212(2):145–156(2002).
- [5] SY. Dhumal, TL. Daulton, J. Jiang, B. Khomami, P. Biswas, "Synthesis of visible light-active nanostructured TiO_x (x\2) photocatalysts in a flame aerosol reactor," *Appl. Catal B*.86(3–4):145–151(2009).
- [6] R. Asahi, T. Morikawa, T. Ohwaki, K. Aoki, Y. Taga, "Visiblelight photocatalysis in nitrogen-doped titanium oxides," *Science* 293(5528):269–271(2001).

7. [7] K. Kardarian, D. Nunes, PM. Sberna, A. Ginsburg, DA. Keller, JV. Pinto, J. Deuermeier, AY. Anderson, A. Zaban, R. Martins, E. Fortunato, "Effect of Mg doping on Cu₂O thin films and their behavior on the TiO₂/Cu₂O heterojunction solar cells," *Sol. Energy Mater Sol Cells* 147:27–36(2016).
8. [8] KP. Priyanka, VR. Revathy, P. Rosmin, B. Thrivedu, KM. Elsa, J. Nimmymol, KM. Balakrishna, T. Varghese,"Influence of La doping on structural and optical properties of TiO₂ nanocrystals. *Mater Charact* 113:144–151(2016).
9. [9] D. Chen, S. Chen, H. Quan, Z. Huang, L. Lu, X. Luo, L. Guo,"Synergetic effects of W⁶⁺ doping and Au modification on the photocatalytic performance of mesoporous TiO₂ clusters. *Adv Powder Technol* 26(6):1590–1596(2015).
10. [10] Y. Cheng, M. Zhang, G. Yao, L. Yang, J. Tao, Z. Gong, G. He, Z. Sun, "Band gap manipulation of cerium doping TiO₂ nanopowders by hydrothermal method. *J. Alloys Compd.* 662:179–184(2016).
11. [11] A. Alem and H. Sarpoolaky, "The effect of silver doping on photocatalytic properties of titania multilayer membranes," *Solid State Sci.* 12, 1469–1472(2010).
12. [12] A. Alem and H. Sarpoolaky, "Synthesis and stabilization of nano-sized titanium dioxide," *Russ. Chem. Rev.*78, 873–885(2009).
13. [13] R. T. Shannon, *Acta. Crystallogr. Sect. A: Cryst. Phys. Diffr. Theor. Gen. Crystallograp.* 32, 751(1976).
14. [14] M. Vishwas M, Sharmar Sudhir Kumar, K. Narashimha Rao, S. Mohan, KV Arjuna. Gowda, RPS. Chakradhar, "Optical, dielectric and morphological studies of sol–gel derived nanocrystalline TiO₂ films," *Spectrochim Acta, Part A* 74:839–842(2009).
15. [15] V. Senthilkumar, M. Jayachandran, C. Sanjeeviraja, "Preparation of anatase TiO₂ thin films for dye-sensitized solar cell by DC reactive magnetron sputtering technique,"*Thin Solid Films* 519:991–994(2010).
16. [16] Kumar PS, Raj AD, Mangalraj D, Nataraj D, "Growth and characterization of ZnO nanostructured thin films by a two step chemical method," *Appl Surf Sci* 255:2382–2387(2008).
17. [17] P. Manurung, Y. Putri, W. Simanjuntak, IM. Low, "Synthesis and characterization of chemical bath deposited TiO₂ thin-films. *Ceram Int* 39:255–259(2013).
18. [18] Raj A .Moses Ezhil, V. Agnes, V. Bena Jothy, C. Sanjeeviraja, "Low temperature TiO₂ rutile phase thin film synthesis by chemical spray pyrolysis [SP] of titanyl acetylacetonate. *Mater Sci Semicond Process* 13:389–394(2010).
19. [19] Hadi, E.H., Abbsa, M.A., Khadayeir, A.A., Abood, Z.M., Habubi, N.F., Chiad, S.S., Effects of Mn doping on the characterization of nanostructured TiO₂ thin films deposited via chemical spray pyrolysis method, *Journal of Physics: Conference Series*, 1664(1), 2020.
20. [20] Chiad, S. S. and Mubarak, T. H.,The Effect of Ti on Physical Properties of Fe₂O₃ Thin Films for Gas Sensor Applications, 2020, *International Journal of Nanoelectronics and Materials*,2020, 13(2), pp. 221-232.
21. [21] Sakhil, M.D., Shaban, Z.M., Sharba, K.S., Habub, N.F., Abass, K.H., Chiad, S.S., Alkelaby, A.S., Influence mgo dopant on structural and optical properties of nanostructured cuo thin films, *NeuroQuantology*, 18 (5), pp. 56-61, 2020.
22. [22] Al Rawas, A.S., Slewa, M.Y., Bader, B.A., Habubi, N.F., Chiad, S.S., Physical characterization of nickel doped nanostructured TiO₂ thin films, *Journal of Green Engineering*10 (9), pp. 7141-7153, 2020.
23. [23] Y.S. Peng, F. Jiang, G. Lu, S. Li, "Effect of doping TiO₂ with alkaline-earth metal ions on its photocatalytic activity," *J. Serb. Chem. Soc.* 72, 393–402(2007). [20] R.S. Dubey, Shyam Singh, "Investigation of structural and optical properties of pure and chromium doped TiO₂ nanoparticle prepared by solvothermal method," *Results, Phys.* 7, 1283–1285(2017).
24. [24] A. Dorian, H. Hanaor and C. Sorrell Charles, "Review of the anatase to rutile phase transformation," *Journal of Materials Science* 46(4):855-874(2011).
25. [25] LG. Devi, R. Kavitha R, "Review on modified N-TiO₂ for green energy applications under UV/visible light: selected results and reaction mechanisms," *RSC, Adv.*4:28265–28299(2014).
26. [26] E. M. Mahdi, M. M. Hamdi, M. Yosoff and P. Wilfred, "XRD and EDXRF Analysis of Anatase Nano-TiO₂ Synthesized from Mineral Precursors", *Adv. Mater. Res.*620,179–185(2013).
27. [27] Khadayeir, A. A., Hassan, E. S., Mubarak, T. H., Chiad, S.S., Habubi, N. F., Dawood, M.O., Al-Baidhany, I. A., The effect of substrate temperature on the physical properties of copper oxide films, *Journal of Physics: Conference Series*, 2019, 1294 (2).
28. [28] Habubi, N.F., Oboudi, S.F., Chiad, S.S., Study of some optical properties of mixed SnO₂-CuO Thin Films, 2012, *Journal of Nano- and Electronic Physics* 4(4) ,04008 (4).
29. [29] Muhammad, S. K., Hassan, E.S., Qader, K.Y., Abass, K.H., Chiad, S. S., Habubi, N. F., Effect of vanadium on structure and morphology of SnO₂ thin films, *Nano Biomedicine and Engineering*, 12(1), pp. 67-74, 2020.
30. [30] Hassan, E.S., Elttayef, A.K., Mostafa, S.H., Salim, M.H., Chiad, S.S., Silver oxides nanoparticle in gas sensors applications, *Journal of Materials Science: Materials in Electronics* 30 (17), pp. 15943-15951, 2019.
31. [31] Chiad, S.S., Noor, H.A., Abdulmunem, O.M., Habubi, N.F., Optical and structural properties of Ni-doped Co₃O₄Nanostructure thin films via CSPM, *Journal of Physics: Conference Series* 1362(1), 2019.
32. [32] Chiad, S.S., Habubi, N.F., Abass, W.H., Abdul-Allah, M.H., Effect of thickness on the optical and dispersion parameters of Cd_{0.4}Se_{0.6} thin films, *Journal of Optoelectronics and Advanced Materials*, 18(9-10), pp. 822-826, 2016.
33. [33] Othman, M.S., Mishjil, K.A., Rashid, H.G., Chiad, S.S., Habubi, N.F., Al-Baidhany, I.A., Comparison of the structure, electronic, and optical behaviors of tin-doped CdO alloys and thin films, *Journal of Materials Science: Materials in Electronics* 31(11), pp. 9037-9043, 2020.

34. [36] Jandow, N.N., Othman, M.S., Habubi, N.F., Chiad, S.S., Mishjil, K.A., Al-Baidhany, I.A., Theoretical and experimental investigation of structural and optical properties of lithium doped cadmium oxide thin films, *Materials Research Express* 6(11), 2020.
35. [37] Ghazai, A.J., Abdulmunem, O.M., Qader, K.Y., Chiad, S.S., Habubi, N.F., Investigation of some physical properties of Mn doped ZnS nano thin films, 2020, *AIP Conference Proceedings* 2213 (1) , 020101.
36. [38] Ali, R.S., Sharba, K.S., Jabbar, A.M., Chiad, S.S., Abass, K.H., Habubi, N.F., Characterization of ZnO thin film/p-Si fabricated by vacuum evaporation method for solar cell applications, 2020, *NeuroQuantology* 18(1), pp. 26-31.
37. [39] M. C. Ju, S. U. Park and J. H. Koh, "Comparative studies of Al-doped ZnO and Ga-doped ZnO transparent conducting oxide thin films," *Nanoscale Res. Lett.* 7, 639(2012).
38. [40] N. N. Jandow, N. F. Habubi, S. S. chiad, I. A. Al-Baidhany and M. A. Qaeed, Annealing Effects on Band Tail Width, Urbach Energy and Optical Parameters of Fe₂O₃:Ni Thin Films Prepared by Chemical Spray Pyrolysis Technique, *International Journal of Nanoelectronics and Materials*, Malaysia, Jan 2019, Volume 12, No. 1, PP. (1-10).
39. [41] Ahmed, F.S., Ahmed, N.Y., Ali, R.S., Habubi, N.F., Abass, K.H. and Chiad, S.S. Effects of Substrate Type on Some Optical and Dispersion Properties of Sprayed CdO Thin Films, *NeuroQuantology*, 18 (3), 56-65, 2020.
40. [42] Chiad, S.S., Alkelaby, A.S., Sharba, K.S., Optical Conduct of Nanostructure Co₃O₄ rich Highly Doping Co₃O₄: Zn alloys, *Journal of Global Pharma Technology*, 11(7), pp. 662-665, 2020
41. [43] I. Soumahoro, R. Moubaaah, G. Schmerber, S. Colis, M. Ait Aouaj, M. Abdlefdil, N. Hassanain, A. Berrada Dinia, *Thin Solid Films* 518, 4593 (2010).
42. [44] P. P. Banerjee, *Proc. IEEE* 73, 1859(2005).
43. [45] Abdulmunem, O.M., Jabbar, A.M., Muhammad, S.K., Dawood, M.O., Chiad, S.S., Habubi, N.F., Investigation of Co-doped Cu₂O thin films on the structural, optical and morphology by SPT, *Journal of Physics: Conference Series* 1660(1), 2020.
44. [46] S. Aksay and B. Altiokka, "Effect of substrate temperature on some of the optical parameters of CuInS₂ films," *Phys. Sta. Sol. (c)* 4, (2) 585-588(2007).
45. [47] M. Vishwas, "Optical properties of Al-doped TiO₂ thin films," *International Journal of Engineering, Science and Mathematics* 6 135(2017).
46. [48] N.Tigau, V.Ci7upina, G. I. Rusu, G. Prodan and E.Vasile , "influence of substrate temperature on the structural and optical properties of Sb₂S₃ thin films," *Rom. J. Phys. Vol. 50 No.7-8*, p859-868(2005).
47. JALIL, A. T., DILFY, S. H., KAREVSKIY, A., & NAJAH, N. (2020). Viral Hepatitis in Dhi-Qar Province: Demographics and Hematological Characteristics of Patients. *International Journal of Pharmaceutical Research*, 12(1). <https://doi.org/10.31838/ijpr/2020.12.01.326>
48. Dilfy, S. H., Hanawi, M. J., Al-bideri, A. W., & Jalil, A. T. (2020). Determination of Chemical Composition of Cultivated Mushrooms in Iraq with Spectrophotometrically and High Performance Liquid Chromatographic. *Journal of Green Engineering*, 10, 6200-6216.
49. Jalil, A. T., Al-Khafaji, A. H. D., Karevskiy, A., Dilfy, S. H., & Hanan, Z. K. (2021). Polymerase chain reaction technique for molecular detection of HPV16 infections among women with cervical cancer in Dhi-Qar Province. *Materials Today: Proceedings*. <https://doi.org/10.1016/j.matpr.2021.05.211>
50. Jalil, A. T., Kadhum, W. R., Khan, M. U. F., Karevskiy, A., Hanan, Z. K., Suksatan, W., ... & Abdullah, M. M. (2021). Cancer stages and demographical study of HPV16 in gene L2 isolated from cervical cancer in Dhi-Qar province, Iraq. *Applied Nanoscience*, 1-7. <https://doi.org/10.1007/s13204-021-01947-9>
51. Widjaja, G., Jalil, A. T., Rahman, H. S., Abdelbasset, W. K., Bokov, D. O., Suksatan, W., ... & Ahmadi, M. (2021). Humoral Immune mechanisms involved in protective and pathological immunity during COVID-19. *Human Immunology*. <https://doi.org/10.1016/j.humimm.2021.06.011>
52. Moghadasi, S., Elveny, M., Rahman, H. S., Suksatan, W., Jalil, A. T., Abdelbasset, W. K., ... & Jarahian, M. (2021). A paradigm shift in cell-free approach: the emerging role of MSCs-derived exosomes in regenerative medicine. *Journal of Translational Medicine*, 19(1), 1-21. <https://doi.org/10.1186/s12967-021-02980-6>
53. Hanan, Z. K., Saleh, M. B., Mezal, E. H., & Jalil, A. T. (2021). Detection of human genetic variation in VAC14 gene by ARMA-PCR technique and relation with typhoid fever infection in patients with gallbladder diseases in Thi-Qar province/Iraq. *Materials Today: Proceedings*. <https://doi.org/10.1016/j.matpr.2021.05.236>
54. Saleh, M. M., Jalil, A. T., Abdulkereem, R. A., & Suleiman, A. A. Evaluation of Immunoglobulins, CD4/CD8 T Lymphocyte Ratio and Interleukin-6 in COVID-19 Patients. *TURKISH JOURNAL of IMMUNOLOGY*, 8(3), 129-134. <https://doi.org/10.25002/tji.2020.1347>
55. Turki Jalil, A., Hussain Dilfy, S., Oudah Meza, S., Aravindhan, S., M Kadhim, M., & M Aljeboree, A. (2021). CuO/ZrO₂ nanocomposites: facile synthesis, characterization and photocatalytic degradation of tetracycline antibiotic. *Journal of Nanostructures*.
56. Sarjito, Elveny, M., Jalil, A., Davarpanah, A., Alfakeer, M., Awadh Bahajjaj, A. & Ouladsmame, M. (2021). CFD-based simulation to reduce greenhouse gas emissions from industrial plants. *International Journal of Chemical Reactor Engineering*, (), 20210063. <https://doi.org/10.1515/ijcre-2021-0063>

57. Marofi, F., Rahman, H. S., Al-Obaidi, Z. M. J., Jalil, A. T., Abdelbasset, W. K., Suksatan, W., ... & Jarahian, M. (2021). Novel CAR T therapy is a ray of hope in the treatment of seriously ill AML patients. *Stem Cell Research & Therapy*, 12(1), 1-23. <https://doi.org/10.1186/s13287-021-02420-8>
58. Jalil, A. T., Shanshool, M. T., Dilyf, S. H., Saleh, M. M., & Suleiman, A. A. (2021). HEMATOLOGICAL AND SEROLOGICAL PARAMETERS FOR DETECTION OF COVID-19. *Journal of Microbiology, Biotechnology and Food Sciences*, e4229. <https://doi.org/10.15414/jmbfs.4229>
59. Vakili-Samiani, S., Jalil, A. T., Abdelbasset, W. K., Yumashev, A. V., Karpishev, V., Jalali, P., ... & Jadidi-Niaragh, F. (2021). Targeting Wee1 kinase as a therapeutic approach in Hematological Malignancies. *DNA repair*, 103203. <https://doi.org/10.1016/j.dnarep.2021.103203>
60. NGAFWAN, N., RASYID, H., ABOOD, E. S., ABDELBASSET, W. K., AL-SHAWI, S. G., BOKOV, D., & JALIL, A. T. (2021). Study on novel fluorescent carbon nanomaterials in food analysis. *Food Science and Technology*. <https://doi.org/10.1590/fst.37821>
61. Marofi, F., Abdul-Rasheed, O. F., Rahman, H. S., Budi, H. S., Jalil, A. T., Yumashev, A. V., ... & Jarahian, M. (2021). CAR-NK cell in cancer immunotherapy; A promising frontier. *Cancer Science*, 112(9), 3427. <https://doi.org/10.1111/cas.14993>
62. Abosaooda, M., Wajdy, J. M., Hussein, E. A., Jalil, A. T., Kadhim, M. M., Abdullah, M. M., ... & Almashhadani, H. A. (2021). Role of vitamin C in the protection of the gum and implants in the human body: theoretical and experimental studies. *International Journal of Corrosion and Scale Inhibition*, 10(3), 1213-1229. <https://dx.doi.org/10.17675/2305-6894-2021-10-3-22>
63. Jumintono, J., Alkubaisy, S., Yáñez Silva, D., Singh, K., Turki Jalil, A., Mutia Syarifah, S., ... & Derkho, M. (2021). Effect of Cystamine on Sperm and Antioxidant Parameters of Ram Semen Stored at 4° C for 50 Hours. *Archives of Razi Institute*, 76(4), 923-931. <https://dx.doi.org/10.22092/ari.2021.355901.1735>
64. Roomi, A. B., Widjaja, G., Savitri, D., Turki Jalil, A., Fakri Mustafa, Y., Thangavelu, L., ... & Aravindhana, S. (2021). SnO₂: Au/Carbon Quantum Dots Nanocomposites: Synthesis, Characterization, and Antibacterial Activity. *Journal of Nanostructures*.
65. Raya, I., Chupradit, S., Kadhim, M. M., Mahmoud, M. Z., Jalil, A. T., Surendar, A., ... & Bochvar, A. N. (2021). Role of Compositional Changes on Thermal, Magnetic and Mechanical Properties of Fe-PC-Based Amorphous Alloys. *Chinese Physics B*. <https://doi.org/10.1088/1674-1056/ac3655>
66. Chupradit, S., Jalil, A. T., Enina, Y., Neganov, D. A., Alhassan, M. S., Aravindhana, S., & Davarpanah, A. (2021). Use of Organic and Copper-Based Nanoparticles on the Turbulator Installment in a Shell Tube Heat Exchanger: A CFD-Based Simulation Approach by Using Nanofluids. *Journal of Nanomaterials*. <https://doi.org/10.1155/2021/3250058>
67. Raya, I., Chupradit, S., Mustafa, Y., H. Oudaha, K., M. Kadhim, M., Turki Jalil, A., J. Kadhim, A., Mahmudiono, T., Thangavelu, L. (2021). Carboxymethyl Chitosan Nano-Fibers for Controlled Releasing 5-Fluorouracil Anticancer Drug. *Journal of Nanostructures*,